Journal of Molecular Structure 1081 (2015) 96–109

Contents lists available at ScienceDirect

Journal of Molecular Structure

journal homepage: www.elsevier.com/locate/molstruc

Quantum mechanical calculations and spectroscopic (FT-IR, FT-Raman and UV) investigations, molecular orbital, NLO, NBO, NLMO and MESP analysis of 4-[5-(4-methylphenyl)-3-(trifluoromethyl)-1H-pyrazol-1-yl] benzene-1-sulfonamide

P. Govindasamy [a,*], S. Gunasekaran [a,b]

[a] Department of Physics, Karpagam University, Eachanari, Coimbatore 641021, TN, India
[b] Research and Development St. Peter's Institute of Higher Education and Research, St. Peter's University, Avadi, Chennai 600054, TN, India

HIGHLIGHTS

- Experimental FT-IR, FT-Raman and UV–Visible spectra of 4MPTFM1HPB1SA were reported.
- NLO, NBO and NLMO analysis of the title molecule were studied.
- HOMO–LUMO energy surface were plotted to identify the donor and acceptor.
- Molecular electrostatic potential of the title compound was calculated.
- The temperature dependence of the thermodynamic properties was investigated.

GRAPHICAL ABSTRACT

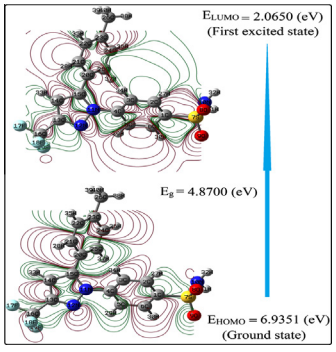

ARTICLE INFO

Article history:
Received 10 August 2014
Received in revised form 3 October 2014
Accepted 7 October 2014
Available online 14 October 2014

Keywords:
4MPTFM1HPB1SA
FT-IR
FT-Raman
NLO
NBO
MESP

ABSTRACT

The molecular structural parameters and vibrational frequencies of the fundamental modes of 4-[5-(4-methylphenyl)-3-(trifluoromethyl)-1H-pyrazol-1-yl] benzene-1-sulfonamide(abbreviated as 4MPTFM1HPB1SA) have been obtained using Density functional theory (DFT) technique in the B3LYP approximation with 6-311G(d,p) and 6-311++G(d,p) basis sets. Detailed vibrational assignments of the observed FT-IR and FT-Raman bands have been proposed on the basis of potential energy distribution (PED). The difference between the observed and the calculated wavenumbers values are very small. The theoretically predicted FT-IR and FT-Raman spectra of the title molecule have been constructed. The molecular electrostatic potential has been mapped primarily for predicting sites and relative reactivities toward electrophilic and nucleophilic attack. The intramolecular contacts have been interpreted using Natural Bond Orbital (NBO) and Natural Localized Molecular Orbital (NLMO) analysis. Important non-linear properties such as electric dipolemoment and first hyperpolarizability of 4MPTFM1HPB1SA have been computed using B3LYP quantum chemical calculation. The absorption wavelength, energy and oscillator's strength are calculated by TD-DFT and 4MPTFM1HPB1SA is approach complement with the experimental findings.

The temperature dependence of thermodynamic properties has been analyzed. The Natural charges, Frontier molecular orbitals (FMOs), chemical hardness (η), chemical potential (μ), Electro negativity (χ) and electrophilicity values (ω) are calculated and reported.

* Corresponding author. Tel.: +91 9976735346.
E-mail address: pgovindasamy1985@gmail.com (P. Govindasamy).

http://dx.doi.org/10.1016/j.molstruc.2014.10.011
0022-2860/

Introduction

4MPTFM1HPB1SA is non-steroidal anti-inflammatory drug (NSAID) which is used to treat inflammatory and painful conditions may be non-selective cyclo-oxygenase (COX) or selective COX-2 inhibitors. Selective COX-2 inhibitors like 4MPTFM1HPB1SA are approved for management of acute pain in adults, treatment of osteoarthritis, rheumatoid arthritis, juvenile rheumatoid arthritis, menstrual cramps, colonic polyps, ankylosing spondylitis and primary dysmenorrhoea.

The 4MPTFM1HPB1SA and its derivatives were studied by several authors. Lavakumar et al. Effect of administration of NSAID on the antidepressant activity have been studied earlier [1]. Chawla et al. solid-state forms were characterized by thermo analytical (DSC, TGA, HSM), crystallographic (XRD), microscopic (polarized, SEM) were investigated [2]. Leonard et al. investigated crystals result in poor blend uniformity, have a tendency to separate out, agglomerate and form a monolithic mass upon compression in the tablet die, making it difficult to process small quantities for formulation were studied [3]. Jozwiakowski et al. Amorphous forms of several drugs (cephalexin, indomethacin, iopanoic acid, frusemide, novobiocin, etc.) have shown enhanced dissolution rates and transient solubility, which translates into greater bioavailability were carried out [4]. Vanden Mooter et al. Techniques that have been used to improve dissolution and bioavailability of poorly water-soluble drugs include micronization, use of surfactants and the formation of solid dispersions were analyzed [5]. Esnaashari et al. studied in the formation of solid dispersions [6]. Salim et al. attempted to design various micro-emulsion formulations of 4MPTFM1HPB1SA for topical and transversal application were carried out [7].

Literature survey reveals that to the best of our knowledge, DFT frequency calculations of the title compound 4MPTFM1HPB1SA have been reported so far. Therefore, the present investigation has been undertaken to study the molecular structure, geometrical parameters, vibrational wavenumbers, modes of vibrations and the Natural Bond Orbital (NBO)/Natural Localized Molecular Orbital (NLMO) analysis which explains the most important orbital interactions in order to classify general structural features. The Natural charge analysis, wavelength, oscillator strength and energies have also been calculated. Furthermore, in order to show nonlinear optic (NLO) activity of title molecule, the dipole moment, polarizability and first hyperpolarizability have also been calculated. Finally, electronegativity (χ), chemical hardness (η) and electrophilicity (ω) of these 4MPTFM1HPB1SA molecules are calculated and interpreted with the use of HOMO and LUMO energies. The local charge distribution analysis and frontier molecular orbitals have been simulated and interpreted. Moreover, molecular electrostatic potential (MESP) surface is plotted over the optimized geometry to explicate the reactivity of 4MPTFM1HPB1SA molecule. The thermodynamic properties of the title compound at different temperature reveal the correlations between standard heat capacities (C), standard entropies (S) and standard enthalpy changes (ΔH).

Experimental

The powder form of 4MPTFM1HPB1SA was procured from leading pharmaceutical company in Chennai and used as such without further purification. Fourier transform infrared spectrum of the title compound is measured at the room temperature recorded in the range 4000–400 cm^{-1} on Bruker IFS 66 V spectrophotometer using KBr pellet technique with 4.0 cm^{-1} resolution. The FT-Raman spectrum recorded using 1064 nm line of Nd:YAG laser as excitation wavelength in the 4000–50 cm^{-1} region on Bruker IFS 66 V spectrophotometer with FRA 106 Raman module which was used as an accessory. The UV–Visible spectral measurements were carried out using a Varian Cary 5E UV–NIR spectrophotometer. The spectral measurements were carried out at Sophisticated Analysis Instrumentation Facility, IIT Madras. India.

Computational details

The molecular geometry optimizations, calculations of energy, vibrational frequencies, IR intensities and Raman activities were carried out for 4MPTFM1HPB1SA with the GAUSSIAN 09W software package [8] using DFT/B3LYP functional combined with the standard 6-311G(d,p) and 6-311++G(d,p) basis sets. DFT employed the B3LYP keyword which invokes Becke's three parameter hybrid method [9] using correlation function of Lee et al. [10]. The optimized structural parameters were used in the vibrational frequency calculations at DFT level to characterize all stationary points as minima. The optimized structural parameters have been evaluated for the calculations of vibrational frequencies by assuming C_1 point group symmetry. The assignment of the calculated wavenumbers was aided by the animation option of Gauss View 5.0 graphical interface from Gaussian programs [11]. Furthermore, the theoretical vibrational spectra of the title compound are interpreted by means of Potential Energy Distribution (PED) using VEDA 4 program [12]. The harmonic frequencies were calculated by B3LYP method using 6-311G(d,p) and 6-311++G(d,p) basis sets. However, the vibrational frequency values computed at this level contain known systematic errors [13,14]. UV–Visible absorption energies, wave length, oscillator strengths of this compound were calculated by TD-DFT method in gas phase, solution DMSO and water. The NBO analysis was performed using the Gaussian 09W package at the B3LYP/6-311++G(d,p) level in order to understand various second order interactions between the filled orbital's of one subsystem and vacant orbital's of another subsystem, which is a measure of the intra-molecular delocalization or hyper conjugation [15]. The Natural charge analyses have been calculated. Finally, in order to show nonlinear optic (NLO) activity of title molecule, the dipole moment, linear polarizability and first hyperpolarizability have also been calculated and hence molecular electrostatic potential (MESP) surface is plotted using DFT method.

Result and discussion

Geometrical structure analysis

The optimized molecular structure of 4MPTFM1HPB1SA belongs to C_1 point group symmetry. The most optimized geometry is performed at B3LYP method with 6-311G(d,p) and 6-311++G(d,p) basis sets of 4MPTFM1HPB1SA molecule with atom numbering scheme is shown in Fig. 1.

The comparative optimized structural parameters such as bond length and bond angle are presented in Table 1. The experimental data on the geometric structure of the related molecule was compared with theoretical values [16]. The N—H bonds found to be shorter than the other bonds of 4MPTFM1HPB1SA. The average bond distances of C—C, C═C, C—H, C—N and C—F calculated by B3LYP method with 6-311G(d,p) and 6-311++G(d,P) basis sets are values 1.3961, 1.3931, 1.0851, 1.3766, 1.3491 and 1.3964, 1.3935, 1.0852, 1.3770, 1.3512 Å respectively. The same optimized C_{15}—C_{20} bond length values are calculated by B3LYP level for 4MPTFM1HPB1SA is 1.4728 and 1.4728 Å using 6-311G(d,p) and 6-311++G(d,p) basis sets respectively. Even the geometrical values calculated with diffuse function, the geometrical parameter values would not be changed as without the same. The computed C_{15}—C_{20} bond length of the title compound value is greater than the experimental value of 1.4710 Å. The calculated double bond lengths

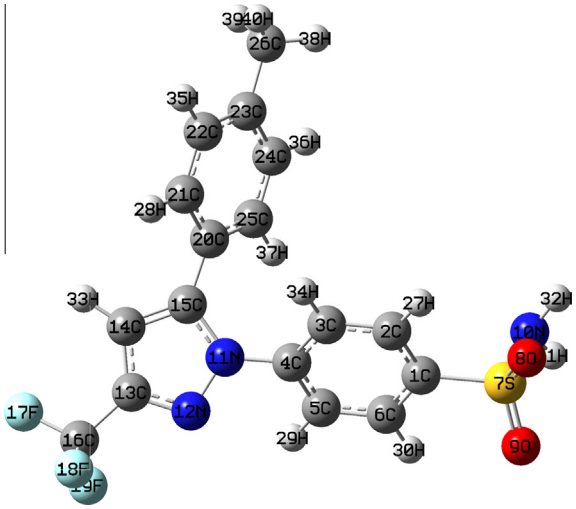

Fig. 1. Structure of 4MPTFM1HPB1SA.

S_7=O_9 and S_7=O_8were found as 1.4586, 1.4589 and 1.4603, 1.4606 Å by B3LYP method with 6-311G(d,p) and 6-311++G(d,p) basis sets, respectively. The calculated C—H bond length values of C_2—H_{27} and C_6—H_{30} are same by B3LYP method with 6-311++G(d,p) basis set. The experimental C—H bond length values are C_2—H_{27}, C_3—H_{34}, C_5—H_{29}, C_6—H_{30}, C_{14}—H_{33}, C_{21}—H_{28}, C_{22}—H_{35}, C_{24}—H_{36} and C_{25}—H_{35} same. The calculated C_1—S_7 bond length is 1.7971 Å and C_5—C_6, C_{20}—C_{21} bond lengths are 1.3895 and 1.4003 Å which are in good agreement with the experimental values.

The calculated bond angles around (F_{17}—C_{16}—F_{18} = 106.8488°, F_{17}—C_{16}—F_{19} = 107.5357°, F_{18}—C_{16}—F_{19} = 106.9554°) and the experimental bond angle values are (F_{17}—C_{16}—F_{18} = 106.4700°, F_{17}—C_{16}—F_{19} = 106.5700°, F_{18}—C_{16}—F_{19} = 107.4800°) indicate the trifluorine ring. The C_{24}—C_{25}—H_{37} bond angle is calculated, the value is 119.5043° by B3LYP/6-311++G(d,p) method and match well with the experimental values [17]. From Table 1, it is found that the bond lengths and bond angles calculated by B3LYP method with 6-311++G(d,p) are consistent with the experimental values. Further the theoretical values, it can be found that most of the optimized bond lengths are slightly higher than the experimental values. The deviations can be attributed to the fact that the theoretical calculations were aimed at the isolated molecules in the gaseous phase and the experimental results were aimed at the molecule in the solid state. Despite these differences, the calculated geometrical parameters represent good approximation and they are the basis for the calculations of other parameters such as vibrational frequencies.

Vibrational assignments

The title molecule 4MPTFM1HPB1SA has 40 atoms, belong to C_1 point group and possess 114 normal vibration modes. The vibrational spectral assignments have been performed based on the recorded FT-IR and FT-Raman spectra and the theoretically predicted wavenumbers of the title molecule. The harmonic vibrational frequencies are calculated for the title compounds by DFT/B3LYP level with 6-311G(d,p) and 6-311++G(d,p) basis sets of theory in order to obtain the spectroscopic signature of the selected compounds. The observed and calculated frequencies using B3LYP level force field along with their probable assignments and potential energy distribution (PED) of the title compound are summarized in Table 2. The observed and simulated FT-IR and FT-Raman spectra of 4MPTFM1HPB1SA compound are shown in Figs. 2

Table 1
Optimized geometrical parameters of 4MPTFM1HPB1SA.

Parameter	B3LYP/6-311G(d,p)	B3LYP/6-311++G(d,p)	Experimental
Bond length (Å)			
C_1—C_2	1.3916	1.3918	1.3770
C_1—C_6	1.3926	1.3927	1.3740
C_1—S_7	1.7963	1.7971	1.7744
C_2—C_3	1.3899	1.3904	1.3850
C_2—H_{27}	1.0822	1.0825	0.9500
C_3—C_4	1.3958	1.3955	1.3780
C_3—H_{34}	1.0812	1.0815	0.9500
C_4—C_5	1.3965	1.3961	1.3780
C_4—N_{11}	1.4255	1.4264	1.4360
C_5—C_6	1.3886	1.3895	1.3870
C_5—H_{29}	1.0813	1.0817	0.9500
C_6—H_{30}	1.0823	1.0825	0.9500
S_7—O_8	1.4589	1.4606	1.4373
S_7—O_9	1.4586	1.4603	1.4283
S_7—N_{10}	1.6902	1.6944	1.6033
N_{10}—H_{31}	1.0143	1.0151	0.8400
N_{10}—H_{32}	1.0143	1.0150	0.8700
N_{11}—N_{12}	1.3519	1.3516	1.3590
N_{11}—C_{15}	1.3817	1.3809	1.3760
N_{12}—C_{13}	1.3228	1.3238	1.3330
C_{13}—C_{14}	1.4070	1.4073	1.3920
C_{13}—C_{16}	1.4967	1.4975	1.4920
C_{14}—C_{15}	1.3827	1.3836	1.3920
C_{14}—H_{33}	1.0766	1.0767	0.9500
C_{15}—C_{20}	1.4728	1.4728	1.4710
C_{16}—F_{17}	1.3526	1.3541	1.3320
C_{16}—F_{18}	1.3499	1.3531	1.3320
C_{16}—F_{19}	1.3448	1.3466	1.3300
C_{20}—C_{21}	1.4002	1.4003	1.3950
C_{20}—C_{25}	1.4018	1.4018	1.3790
C_{21}—C_{22}	1.3913	1.3920	1.3890
C_{21}—H_{28}	1.0841	1.0842	0.9500
C_{22}—C_{23}	1.3977	1.3982	1.3830
C_{22}—H_{35}	1.0850	1.0851	0.9500
C_{23}—C_{24}	1.3999	1.4003	1.3830
C_{23}—C_{26}	1.5086	1.5085	
C_{24}—C_{25}	1.3890	1.3898	1.3820
C_{24}—H_{36}	1.0852	1.0853	0.9500
C_{25}—H_{37}	1.0836	1.0837	0.9500
C_{26}—H_{38}	1.0926	1.0926	
C_{26}—H_{39}	1.0954	1.0955	
C_{26}—H_{40}	1.0918	1.0919	
Bond angle (°)			
C_2—C_1—C_6	121.2916	121.3447	120.7600
C_2—C_1—S_7	119.3359	119.3117	119.8300
C_6—C_1—S_7	119.3688	119.3414	119.4100
C_1—C_2—C_3	119.3736	119.3215	119.5500
C_1—C_2—H_{27}	120.0300	120.1172	120.2000
C_3—C_2—H_{27}	120.5638	120.5374	120.2000
C_2—C_3—C_4	119.6138	119.6018	119.2400
C_2—C_3—H_{34}	120.0458	120.0439	120.4000
C_4—C_3—H_{34}	120.3327	120.3477	120.4000
C_3—C_4—C_5	120.6816	120.7646	121.5500
C_3—C_4—N_{11}	120.7269	120.5234	119.1100
C_5—C_4—N_{11}	118.5482	118.6712	119.3400
C_4—C_5—C_6	119.6982	119.6500	118.7000
C_4—C_5—H_{29}	119.2172	119.4438	120.6000
C_6—C_5—H_{29}	121.0713	120.8969	120.6000
C_1—C_6—C_5	119.3094	119.2846	120.1000
C_1—C_6—H_{30}	120.0484	120.1403	119.9000
C_5—C_6—H_{30}	120.6351	120.5712	119.9000
C_1—S_7—O_8	107.6330	107.5913	107.2200
C_1—S_7—O_9	107.5960	107.5767	106.3200
C_1—S_7—N_{10}	103.1703	103.3904	108.5000
O_8—S_7—O_9	122.7744	122.6453	119.8500
O_8—S_7—N_{10}	106.9253	106.9574	106.3200
O_9—S_7—N_{10}	107.0840	107.0878	108.3600
S_7—N_{10}—H_{31}	110.2657	110.1727	113.6000
S_7—N_{10}—H_{32}	110.1859	110.1131	112.6000
H_{31}—N_{10}—H_{32}	111.8999	111.7102	115.0000
C_4—N_{11}—N_{12}	117.8004	117.9926	117.9500
C_4—N_{11}—C_{15}	129.9253	129.7093	129.3600
N_{12}—N_{11}—C_{15}	112.2057	112.2281	108.5000

Table 1 (*continued*)

Parameter	B3LYP/6-311G(d,p)	B3LYP/6-311++G(d,p)	Experimental
N_{11}—N_{12}—C_{13}	104.8583	104.8466	103.7000
N_{12}—C_{13}—C_{14}	112.2726	112.2749	112.9300
N_{12}—C_{13}—H_{16}	120.0914	119.9486	119.2400
C_{14}—C_{13}—C_{16}	127.6216	127.7594	127.8200
C_{13}—C_{14}—C_{15}	105.0036	104.9355	105.1000
C_{13}—C_{14}—H_{33}	127.9732	128.0844	127.5000
C_{15}—C_{14}—H_{33}	126.9248	126.8796	127.5000
N_{11}—C_{15}—C_{14}	105.6534	105.7078	105.8500
N_{11}—C_{15}—C_{20}	125.8763	125.7502	125.0300
C_{14}—C_{15}—C_{20}	128.3286	128.4167	129.1200
C_{13}—C_{16}—F_{17}	110.3122	110.4446	112.4500
C_{13}—C_{16}—F_{18}	112.1246	112.2171	112.5700
C_{13}—C_{16}—F_{19}	112.3176	112.5424	110.9400
F_{17}—C_{16}—F_{18}	107.0157	106.8488	106.4700
F_{17}—C_{16}—F_{19}	107.7034	107.5357	106.5700
F_{18}—C_{16}—F_{19}	107.1067	106.9554	107.4800
C_{15}—C_{20}—C_{21}	119.7657	119.7560	122.8500
C_{15}—C_{20}—C_{25}	121.8165	121.8138	118.7400
C_{21}—C_{20}—C_{25}	118.3530	118.3702	118.4200
C_{20}—C_{21}—C_{22}	120.6785	120.6702	120.4000
C_{20}—C_{21}—H_{28}	119.4601	119.5245	119.8000
C_{22}—C_{21}—H_{28}	119.8554	119.7993	119.8000
C_{21}—C_{22}—C_{23}	121.2016	121.2076	120.3000
C_{21}—C_{22}—H_{35}	119.2688	119.2436	119.9000
C_{23}—C_{22}—H_{35}	119.5287	119.5480	119.9000
C_{22}—C_{23}—C_{24}	117.8665	117.8526	119.9000
C_{22}—C_{23}—C_{26}	121.2176	121.2201	
C_{24}—C_{23}—C_{26}	120.9031	120.9149	
C_{23}—C_{24}—C_{25}	121.3343	121.3338	120.0000
C_{23}—C_{24}—H_{36}	119.4724	119.4946	120.0000
C_{25}—C_{24}—H_{36}	119.1920	119.1703	120.0000
C_{20}—C_{25}—C_{24}	120.5653	120.5649	121.0000
C_{20}—C_{25}—H_{37}	119.8685	119.9277	119.5000
C_{24}—C_{25}—H_{37}	119.5628	119.5043	119.5000
C_{23}—C_{26}—H_{38}	111.4191	111.4231	
C_{23}—C_{26}—H_{39}	110.8624	110.8278	
C_{23}—C_{26}—H_{40}	111.4458	111.4408	
H_{38}—C_{26}—H_{39}	107.3053	107.3146	
H_{38}—C_{26}—H_{40}	108.1349	108.1593	
H_{39}—C_{26}—H_{40}	107.4839	107.4876	

and 3 respectively. The calculated frequencies are slightly higher than the observed values for the majority of the normal modes. Two factors may be the reason for the discrepancies between the experimental and computed spectra of this compound. The first is the influence of the environment and the second one is the fact that the experimental value is an anharmonic frequency while the calculated value is a harmonic frequency. The calculated harmonic wavenumbers are usually higher than the corresponding experimental quantities because of the combination of electron correlation effects and the basis set deficiencies. The maximum number of values determined by B3LYP/6-311++G(d,p) is in good agreement with the experimental values.

NH_2 vibrations

Primary aliphatic amides absorb in the region 3520-3320 cm^{-1} [18–20]. The position of absorption in this region depends upon the degree of hydrogen bonding and the physical state of the sample or the polarity of the solvent. The NH_2 stretching modes are 3513 and 3509 cm^{-1} (mode no. 2) by B3LYP level with 6-311G(d,p) and 6-311++G(d,p) basis sets, while the experimental values are 3347 and 3520 cm^{-1} in FT-IR and FT-Raman spectrum respectively, are presented in Table 2. The PED contributions are 100% for stretching mode.

C—H vibrations

Most of the aromatic compounds have infrared peaks in the region 3100-3000 cm^{-1} due to ring C—H stretching bonds [21–23]. In our present work, the bands observed at 3098 cm^{-1} in FT-IR and 3116 cm^{-1} in FT-Raman are assigned to C—H stretching vibrations of the title compound. The calculated values of these modes for the title molecule have been found to be 3107 and 3106 cm^{-1} at B3LYP level with 6-311G(d,p) and 6-311++G(d,p) basis sets calculation. As indicated by the PED, these modes involve approximately 83% contribution suggesting that they are stretching modes. The substituted benzene like molecule gives rise to C—H stretching, C—H in-plane and C—H out-of-plane bending. The in-plane C—H bending vibrations appear in the range 1475–1450 cm^{-1} [24] in the substituted benzenes and the out-of-plane bending vibrations occurs in the frequency range 750–1000 cm^{-1} [25]. Accordingly, the calculated frequencies assigned to two C—H in-plane bending vibrations are 1476 and 1473 cm^{-1} for 4MPTFM1HPB1SA, while the bands observed at 1474 cm^{-1} in FT-IR and 1473 cm^{-1} in FT-Raman. The calculated frequencies are 846, 834 and 829 cm^{-1} and observed frequencies are 844, 825 and 809 cm^{-1} assigned to C—H out-of-plane bending vibrations for 4MPTFM1HPB1SA. This also shows good agreement with the experimental values as given in Table 2.

CH_3 vibrations

Methyl groups are generally referred as electron donating substituent's in the aromatic ring system. The C–H stretching in CH_3 occurs at lower frequencies than those of aromatic ring. For CH_3 compound the mode appear in the region 2962–2872 cm^{-1} are assigned to CH_3 stretching mode of vibrations [24,25]. In the present work, the FT-IR bands observed at 2917 and 2858 cm^{-1} and the FT-Raman bands observed at 2917 and 2855 cm^{-1} have been assigned to CH_3 stretching vibrations. [26–28]. The B3LYP level at 6-311G (d,p) and 6-311++G(d,p) basis sets values are 2925, 2847, 2924, 2845 and 2925, 2847, 2924, 2845 cm^{-1} respectively as shown in Table 2. In general, the aromatic CH_3 stretching vibration calculated values are in good agreement with the experimental values. These vibrations are identified as pure mode with 80% of PED values.

C═C and C—C vibrations

The C═C aromatic stretching vibrations give rise to characteristic bonds in both the observed FT-IR and FT-Raman spectra, covering the spectral region ranging from 1650 to 1430 cm^{-1} [29]. In our study the C═C stretching vibrations of the present compound observed at 1612 and 1581 cm^{-1} in FT-IR and 1613 and 1575 cm^{-1} in FT-Raman are assigned to C═C stretching vibrations respectively. These vibrations are identified as pure mode with 53% of PED values. The calculated values are 1626, 1588 and 1625, 1584 cm^{-1} by B3LYP methods with 6-311G(d,p) and 6-311++G(d,p) basis sets respectively. The ring C—C stretching vibrations normally occur in the region 1590–1430 cm^{-1} [30]. The present case C—C stretching vibrations have been observed at 1446 cm^{-1} in FT-IR and the very strong band observed at 1445 cm^{-1} in FT-Raman is due to C—C stretching vibrations. These vibrations are identified with the PED values. The calculated wavenumbers are 1442 and 1440 cm^{-1} by B3LYP methods with 6-311G(d,p) and 6-311++G(d,p) basis sets respectively. The C═C and C—C stretching vibrations predicted by B3LYP with 6-311++G(d,p) basis set values are in good agreement with the experimental values as presented in Table 2. The bands are observed at 1045, 1020, 801 and 620 cm^{-1} in FT-IR and 1032, 793 and 645 cm^{-1} in FT-Raman have been assigned to C—C in plane bending vibrations. The C—C out-of-plane bending vibration is found at 347 cm^{-1} in FT-Raman. The C—C torsion vibrations are observed at 970, 743 and 721 cm^{-1} in FT-IR and 971, 742 and 419 cm^{-1} in FT-Raman.

C—N vibrations

The identification of C—N vibration is a very difficult task, since the mixing of several bands is possible in this region. The C—N stretching vibrations generally occur in the region

Table 2
Vibrational band assignments of 4MPTFM1HPB1SA.

Mode no.	Experimental wavenumber (cm^{-1})		Calculated wavenumber (cm^{-1})		Vibrational band assignment with (% PED)
	υ(IR)	υ(Raman)	B3LYP/6-311G(d,p)	B3LYP/6-311++G(d,p)	
1			3621	3616	υNH_2(100)
2	3347s	3520vw	3513	3509	υNH_2(100)
3	3241s	3240vw	3262	3260	υCH(99)
4		3216vw	3219	3216	υCH(99)
5		3206vw	3218	3215	υCH(91)
6			3204	3202	υCH(99)
7		3196vw	3203	3201	υCH(100)
8			3186	3185	υCH(89)
9		3175vw	3183	3182	υCH(89)
10			3162	3162	υCH(82)
11	3153w	3147vw	312	3162	υCH(79)
12	3098w	3116vw	3107	3106	υCH(83)
13	2917vw	2917w	2925	2924	υCH_3(63)
14	2858w	2855w	2847	2845	υCH_3(80)
15			1656	1653	υCC(38)
16			1637	1634	υCC(44)
17	1612vw	1613vs	1626	1625	υCC(53) + δCCC(14)
18			1606	1604	υCC(21)
19	1590w	1595vw	1593	1587	δHNH(78) + τHNSC(11)
20	1581w	1575vw	1588	1584	υCC(38)
21	1550vw	1549s	1548	1544	υNC(14) + δHCC(10)
22		1520w	1529	1528	δHCC(24)
23	1498w	1497vw	1497	1495	δHCH(56)
24			1492	1490	δHCC(16)
25			1489	1485	δCNN(15)
26	1474m	1473vw	1476	1473	υNC(79) + δHCC(18)
27	1446m	1445vs	1442	1440	υCC(44)
28			1437	1435	δCCC(23)
29	1402w	1414vw	1417	1416	υHCH(42)
30	1374m	1374vw	1383	1382	υNC(25) + δHCH(21)
31	1347vs	1345vw	1346	1342	υHCH(23)
32	1332w		1340	1340	υNN(20)
33			1329	1329	δHCC(19)
34	1314w	1316vw	1326	1316	υSO_2(31)
35			1314	1313	υSO2(28)
36	1274s	1273vw	1288	1286	υCN(21)
37			1251	1245	υCC(12) + δHCC(21)
38	1229vs	1227vw	1235	1234	υNN(36)
39			1219	1217	υCC(13) + υNN(25)
40			1210	1210	δHCC(16)
41	1197w	1193w	1201	1201	υCC(10) + δHCC(23)
42			1169	1144	υFC(17)
43		1136vw	1152	1142	υCF3(56)
44	1135vs		1143	1134	δCCC(10)
45		1133vw	1135	1128	υSO(23)
46			1133	1120	υFC(32)
47	1103s	1094vw	1114	1109	υCF3(23)
48	1093s		1088	1091	δHCC(20)
49			1087	1085	δHCC(16)
50			1082	1078	υCC(15) + υCS(15)
51	1063vw	1061vw	1063	1061	τHCCC(44)
52	1045v		1039	1039	δCCC(14)
53	1020w	1032vw	1032	1031	δCCC(39)
54			1009	1008	δHCH(12)
55			993	995	τHCCC(35)
56			989	990	δNNC(19)
57			988	985	δCCC(12)
58	981w	981vw	981	985	τHCCC(14)
59			975	978	τHCCC(16) + τHCCN(12) + τCCCC(10)
60	970w	971vw	971	969	τHCCC(20) + τCCCC(12)
61			861	861	τHCCC(16) + τHCCN(19)
62			856	851	τHCCC(13)
63	846m		853	849	υSN(37) + τHNSC(13)
64			851	846	τHCCC(20) + τHCCN(24)
65		844vw	846	846	γHCCC(15) + τHCCN(18)
66	825w	809vw	834	829	τHCCN(42) + γHCCC(13)
67	801w	793vw	813	812	δCCC(10)
68	762w	761vw	762	761	υCS(21)
69	743vw	742vw	742	740	τCCCC(17)
70		726vw	740	736	δCCF(10)
71			738	734	τHCCN(10)
72	721vw		730	733	τCCCC(18)
73		708vw	704	703	τCCNC(13)

Table 2 (*continued*)

Mode no.	Experimental wavenumber (cm^{-1})		Calculated wavenumber (cm^{-1})		Vibrational band assignment with (% PED)
	υ(IR)	υ(Raman)	B3LYP/6-311G(d,p)	B3LYP/6-311++G(d,p)	
74	648w	674vw	655	654	δCCC(23)
75		645vw	642	641	δCCC(24)
76	633m		635	636	υSN(27) + τHNSC(18)
77	620w		629	629	δCCC(14)
78			616	615	δCCC(14)
79	586vw		586	585	υCS(31)
80	561w	562vw	566	564	γFCFC(10)
81			558	556	δFCF(10)
82	532m		538	537	γFCFC(20)
83	512w	510vw	515	513	δFCF(16)
84	497vw		493	492	δFCF(13)
85	480vw		470	471	δOSO(24)
86		442vw	441	441	δOSO(15)
87			434	433	γONCS(13)
88		419vw	422	422	τCCCC(29)
89			416	415	τHCCC(11)
90			414	412	δFCF(17)
91			379	378	δCCC(34)
92			372	371	δOSN(31)
93		357vw	360	358	δOSO(15) + δOSN(10)
94		347vw	351	349	γCCCC(12)
95		324vw	338	337	δFCF(13) + δCCC(12)
96			293	292	δCCC(11) + δNCC(12)
97		251vw	262	261	δNSC(19)
98			239	238	υCC(20)
99		204vw	207	206	δNSC(12)
100			199	198	δSNH(12)
101		178vw	175	176	δSNH(16)
102			146	150	δSCC(10)
103			137	141	δOSN(15) + τHNSC(18)
104			119	135	γCCNC(17)
105		102vs	106	104	γSCCC(12)
106		72vs	91	91	γSCCC(16)
107			63	63	δCCN(15)
108			55	54	τCCCC(20) + τCNCC(17)
109			44	45	τCCNC(34)
110			42	43	τNSCC(19)
111			38	38	τCCCN(42)
112			28	27	δCN(16) + τCCCC(11)
113			20	22	τNCC(29) + τNSCC(48)
114			18	17	τCFFF(91)

m – medium; w – weak; s – strong; vw – very weak; vs – very strong; υ – stretching; δ – bending; γ – Out of plane bending; τ – torsion; potential energy distribution (PED).

1180–1280 cm^{-1} [24]. The C—N stretching vibration strong band observed at 1274 in FT-IR and very weak at 1273 cm^{-1} in FT-Raman are assigned to C—N stretching vibrations. James et al. [31] assigned 1370 cm^{-1} for 1-benzyl-1-H-imidazole for C—N vibration. Pinchaset et al. [32] assigned the C—N stretching at 1368 cm^{-1} in benzamide. Kahovec and Kohlreusch et al. [33] identified the stretching wavenumber of C—N band in salicylicaldoxinne at 1617 cm^{-1}. In the present investigation the bands observed at 1550, 1474 and 1374 cm^{-1} in FT-IR and 1549, 1473 and 1374 cm^{-1} in FT-Raman are assigned to C—N stretching vibration as given in Table 2.

The theoretically calculated value of C—N stretching vibrations are 1548, 1476, 1383 and 1544, 1473, 1382 cm^{-1} by B3LYP level with 6-311G(d,p) and 6-311++G(d,p) basis sets respectively. The C–N torsion vibration observed at 708 cm^{-1} in FT-IR for 4MPTFM1HPB1SA.

N—N vibrations

The N—N stretching absorption is found in the region 1332, 1227 and 1229 cm^{-1} [34]. The weak band is observed at 1332 $cm^{-1}$and very strong band is observed at 1229 cm^{-1} in FT-IR and 1227 cm^{-1} in FT-Raman are assigned to N—N stretching mode. The calculated wavenumber values of the mentioned mode were found as 1340, 1235 and 1340, 1234 cm^{-1} by B3LYP method with 6-311G(d,p) and 6-311++G(d,p) basis sets respectively are presented in Table 2.

SO_2 vibrations

The SO_2 stretching vibrations are appearing in the range of 1335–1295 cm^{-1} [24]. The observed bands are 1314 and 1316 cm^{-1} in the FT-IR, and FT-Raman spectrum respectively. The calculated SO_2 stretching modes are 1326 and 1316 cm^{-1} [35–37]. The out-of-plane bending vibrations for the title molecule are found at 480 cm^{-1} in FT-IR and 442 and 357 cm^{-1} in FT-Raman. The theoretically computed frequencies for SO_2 vibrations show an excellent agreement with the recorded spectrum as well as the literature values. All the SO_2 vibrational bands of the title compound are in line with the literature values and nearly in agreement with the computed values by B3LYP/6-311++G(d,p) as given in Table 2.

S═O Vibrations

Solutions of sulfonamide absorb strongly at 1170–1155 cm^{-1} [24] and 1245–1155 cm^{-1} [18]. In solid phase these frequencies are lower by 10–20 cm^{-1}. In the present investigation, a band observed at 1133 cm^{-1} in FT-Raman is due to S═O stretching vibration. The theoretically calculated values are 1135 and 1128 cm^{-1} by B3LYP method with 6-311G(d,p) and

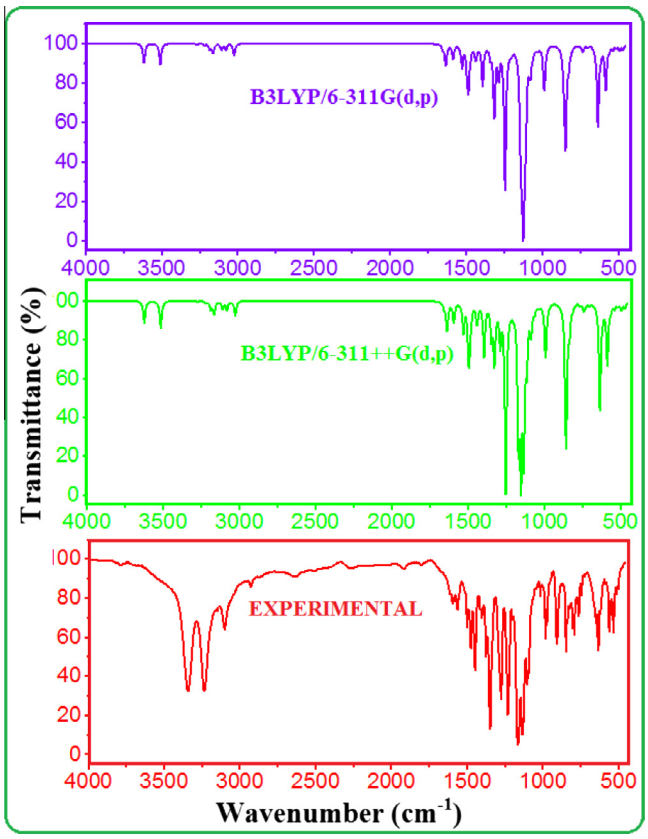

Fig. 2. Experimental and simulated FT-IR spectra of 4MPTFM1HPB1SA.

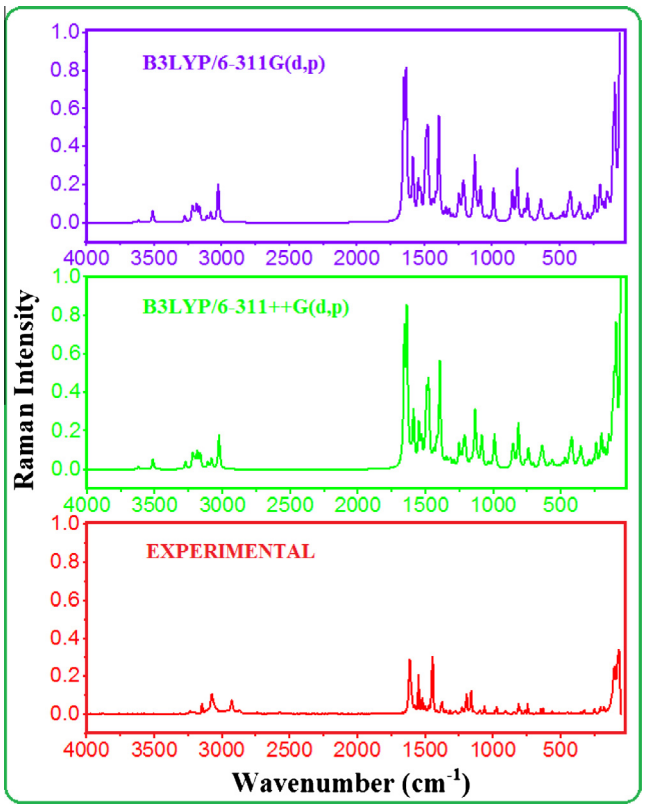

Fig. 3. Experimental and simulated Raman spectra of 4MPTFM1HPB1SA.

6-311++G(d,p) basis sets respectively also shows good agreement with the experimentally recorded data as presented in Table 2.

CF_3 vibrations

The trifluoromethyl group (CF_3) has a set of fairly well defined group frequencies associated with it. The highest frequency fundamental vibration of the CF_3 group is the CF_3 stretch which occurs between 1350 and 1120 cm^{-1} [24]. These vibrational motions were observed to give rise to extremely intense infrared absorption and rather weak Raman. The CF_3 stretching vibrations are observed at 1136 and 1094 cm^{-1} in FT-Raman and strong band found at 1103 cm^{-1} in FT-IR for 4MPTFM1HPB1SA [38–40]. The CF in-plane bending mode is observed at 510 cm^{-1} in FT-Raman and 512 and 497 cm^{-1} in FT-IR for 4MPTFM1HPB1SA. These vibrational modes are also confirmed by their PED values. The CF out-of-plane bending modes are found at 561 and 532 cm^{-1} in FT-IR and 562 cm^{-1} in FT- Raman for 4MPTFM1HPB1SA. The CF out-of-plane modes were calculated at 566, 538 and 564, 537 cm^{-1} by using B3LYP level with 6-311G(d,p) and 6-311++G(d,p) basis sets respectively are presented in Table 2.

S—N vibrations

The S—N stretching vibration [35] is expected in the region 905 ± 30 cm^{-1}. The S—N stretching vibration is observed in the region 846 and 633 cm^{-1}. The medium bands are observed at 846 cm^{-1} in FT-IR and 633 cm^{-1} in FT-Raman. The calculated wavenumbers are 853, 635, 849 and 636 cm^{-1} are assigned to S—N stretching mode for our title molecule as given in Table 2. The theoretically calculated values show good correlation with the experimental observations.

C—S vibrations

In general, the assignment of the band due to C—S stretching vibrations in different compounds is difficult. Because of the mixing of several bands, the identification of C—S vibrations is a very difficult task. The stretching vibrations assigned to the C—S linkage assigned to in region of occur in the region 700–600 cm^{-1} [18] and 775–650 cm^{-1} [24]. The band observed at 762 and 586 cm^{-1} in FT-IR and 761 cm^{-1} in FT-Raman are assigned to C—S stretching modes of vibration [41]. The PED for this mode suggests that this is a pure mode. The calculated wavenumbers are 762, 586 and 762, 585 cm^{-1} by B3LYP level with 6-311G(d,p) and 6311++G(d,p) basis sets respectively.

The calculated wavenumbers are good agreement with the experimental data. The out-of-plane bending vibrations are found at 102 and 72 cm^{-1} in FT-Raman. The theoretically calculated values are 106, 91 and 104, 91 cm^{-1} by B3LYP level with 6-311G(d,p) and 6-311++G(d,p) basis sets respectively and the values are in good agreement with the experimental values as presented in Table 2.

Non-linear optical properties

Nonlinear optical (NLO) effects arise from the interactions of electromagnetic fields in various media to produce new fields altered in phase, frequency, amplitude or other propagation characteristics from the incident fields [42]. The results of the calculated molecular polarizabilities at DFT/B3LYP/6-311++G(d,p) level on the basis of the finite-field approach are given in Table 3. By considering Table 3, the values of the second-order polarizability or first hyperpolarizability (β), dipole moment (μ) and polarizability (α) of title molecule are reported in the atomic mass units (a.u) and electrostatic unit (esu). First hyperpolarizability is a third rank tensor that can be described by a $3 \times 3 \times 3$ matrix. The 27 components of the 3D matrix can be reduced to 10 components due to the

Table 3
The calculated μ_{tot}, α_0 and β_o components 4MPTFM1HPB1SA.

Parameters	Value	esu ($\times 10^{-24}$)	Parameters	Value	esu ($\times 10^{-33}$)
α_{xx}	291.0269	43.1302	β_{xxx}	549.5709	−4747.9079
α_{xy}	−0.8884	−0.1317	β_{xxy}	−36.0175	−311.1662
α_{yy}	273.6928	40.5613	β_{xyy}	28.1231	242.9640
α_{xz}	−11.3997	−1.6894	β_{yyy}	−41.9404	−362.3358
α_{yz}	−14.4548	−2.1422	β_{xxz}	−23.8379	−205.9427
α_{zz}	176.9115	26.2183	β_{xyz}	−21.5927	−186.5458
α_0	247.2104	36.6366	β_{yyz}	−26.1779	−226.1585
$\Delta\alpha$	609.4845	90.3256	β_{xzz}	37.3703	322.8531
μ_x	−0.2896		β_{yzz}	48.4529	418.5987
μ_y	1.1338		β_{zzz}	−38.7076	−334.4065
μ_z	−0.6485		β_o	493.0247	4259.3883
μ_{tot}	1.3378				

Kleinman symmetry [43]. It can be given in the lower tetrahedral format. It is obvious that the lower part of the $3 \times 3 \times 3$ matrices is a tetrahedral. The components of β are defined as the coefficients in the Taylor series expansion of the energy in the external electric field. When the external electric field is weak and homogeneous, this expansion becomes:

$$E = E^0 - \mu_\alpha F_\alpha - 1/2\alpha_{\alpha\beta}F_\alpha F_\beta - 1/6\beta_{\alpha\beta\gamma}F_\alpha F_\beta F_\gamma + \ldots$$

where E^0 is the energy of the unperturbed molecules, F_α is the field at the origin μ_α, $\alpha_{\alpha\beta}$ and $\beta_{\alpha\beta\gamma}$ are the components of dipole moment, polarizability and the first order hyperpolarizabilities respectively.

In Gaussian 09W output, the complete equations for calculating the magnitude of total static dipole moment (μ_{tot}), the mean polarizability (α_o), the anisotropy of the polarizability ($\Delta\alpha$) and the mean first hyperpolarizability (β_o) by using the x, y, z components they are defined as follows: [44,45].

The mean polarizability is defined as,

$$\alpha_0 = \frac{\alpha_{xx} + \alpha_{yy} + \alpha_{zz}}{3}$$

The polarizability anisotropy invariant is

$$\Delta\alpha = \frac{1}{\sqrt{2}} \times \sqrt{(\alpha_{xx} + \alpha_{yy})^2 + (\alpha_{yy} + \alpha_{zz})^2 + (\alpha_{zz} + \alpha_{xx})^2 + 6\alpha_{xz}^2 + 6\alpha_{xy}^2 + 6\alpha_{yz}^2}$$

The components of the first hyperpolarizability can be calculated using the following equation. Using the x, y and z components of β the magnitude of the first hyperpolarizability tensor can be calculated by:

$$\beta_0 = \sqrt{(\beta_x^2 + \beta_y^2 + \beta_z^2)}$$

The complete equation for calculating the magnitude of β_0 from Gaussian 09W output is given as follows:

$$\beta_0 = \sqrt{(\beta_{xxx} + \beta_{xyy} + \beta_{xzz})^2 + (\beta_{yyy} + \beta_{yzz} + \beta_{yxx})^2 + (\beta_{zzz} + \beta_{zxx} + \beta_{zyy})^2}$$

$$\beta_x = \beta_{xxx} + \beta_{xyy} + \beta_{xzz}$$

$$\beta_y = \beta_{yyy} + \beta_{yzz} + \beta_{yxx}$$

$$\beta_z = \beta_{zzz} + \beta_{zxx} + \beta_{zyy}$$

In Table 3, the calculated parameters described above and electronic dipole moment {μ_i (i = x, y, z) and total dipole moment μ_{tot}} for title compound were listed.

The total dipole moment can be calculated using the following equation.

$$\mu_{tot} = \sqrt{(\mu_x^2 + \mu_y^2 + \mu_z^2)}$$

It is well known that the higher values of dipole moment, molecular polarizability and hyperpolarizability are important for more active NLO properties. The polarizabilities and hyperpolarizability are reported in atomic units (a.u), the calculated values have been converted into electrostatic units (esu) (for α; 1 a.u = 0.1482×10^{-24} esu, for β; 1 a.u = 8.6393×10^{-33} esu). The highest value of dipole moment is observed for component μ_y. In this direction, the value is equal to 1.1338 Debye. The lowest value of the dipole moment of the 4MPTFM1HPB1SA compound is μ_z component (−0.6485). Urea is one of the prototypical molecules used in the study of the NLO properties of molecular systems. Therefore it was used frequently as a threshold value for comparative purposes. The total molecular dipole moment (μ_{tot}) and the first order hyperpolarizability are 1.3378 Debye and $4.259.3883 \times 10^{-30}$ esu respectively and are depicted in Table 3. Total dipole moment of title molecule is nearly equal to urea and the first order hyperpolarizability of title molecule greater than that of urea (μ_{tot} and β_0 urea are 1.5256 Debye and 0.7803×10^{-30} esu [46] respectively, obtained by B3LYP/6-311++G(d,p) method.

NBO and NLMO analysis

Natural Bond Orbital (NBO) analysis provides an efficient method for studying interesting features of molecular structure. They give strong insight in the intra and inter molecular bonding and interaction among bonds and also provide a convenient basis for investigation of charge transfer or conjugative interactions in molecular system. Another useful aspect of NBO method is that it gives information about interactions in both filled and virtual orbital spaces that could enhance the analysis of intra and intermolecular interactions. The second order Fock matrix was carried out to evaluate the donor–acceptor interactions in the NBO analysis [47–49]. The interactions result in a loss of occupancy from the localized NBO of the idealized Lewis structure into an empty non-Lewis orbital.

For each donor NBO (i) and acceptor NBO (j), the stabilization energy associated with $i \rightarrow j$ delocalization can be estimated as,

$$E^{(2)} = \Delta E_{ij} = q_i \frac{F_{(i,j)}^2}{\varepsilon_j - \varepsilon_i}$$

where q_i is the donor orbital occupancy, ε_j and ε_i are diagonal elements and $F_{(i,j)}$ is the off diagonal NBO Fock matrix element [50] In NBO analysis large $E(2)$ value shows the intensive interaction between electron donors and electron-acceptors and greater the extent of conjugation of the whole system, the possible intensive interactions are given in Table 4 as supporting information. The second-order perturbation theory analysis of Fock matrix in NBO basis shows strong intra-molecular hyper-conjugative interactions of π electrons. In 4MPTFM1HPB1SA, the interactions $\pi^*(C_{20}—C_{25}) \rightarrow \pi^*(C_{23}—C_{24})$ have the highest E(2) value around 271.050 kcal/mol.

Table 4
NBO analysis of 4MPTFM1HPB1SA.

Type	Donor NBO (*i*)	Type	Acceptor NBO (*j*)	$E^{a}(2)$ (kcal/mol)	$E(j)-E(i)^{b}$ (a.u)	$F(i,j)^{c}$ (a.u)
π	C_1—C_6	π*	C_2—C_3	21.760	0.290	0.071
π	C_2—C_3	π*	C_4—C_5	22.150	0.270	0.070
σ	C_4—C_5	σ*	C_1—C_6	23.040	0.270	0.071
σ	N_{12}—C_{13}	σ*	C_{14}—C_{15}	13.220	0.330	0.062
π	C_{14}—C_{15}	π*	N_{12}—C_{13}	29.840	0.250	0.081
σ	C_{20}—C_{25}	σ*	C_{21}—C_{22}	19.970	0.280	0.067
σ	C_{21}—C_{22}	π*	C_{23}—C_{24}	20.780	0.280	0.069
σ	C_{23}—C_{24}	π*	C_{20}—C_{25}	23.380	0.270	0.071
	LP(2)O_8	σ*	C_1—S_7	12.550	0.320	0.057
	LP(3)O_8	σ*	S_7—O_9	16.790	0.310	0.064
	LP(2)O_9	σ*	C_1—S_7	12.500	0.320	0.057
	LP(3)O_9	σ*	S_7—O_8	16.660	0.310	0.064
	LP(1)N_{11}	π*	C_{14}—C_{15}	34.470	0.300	0.093
	LP(2)F_{17}	σ*	C_{16}—F_{18}	12.890	0.540	0.075
	LP(3)F_{18}	σ*	C_{16}—F_{17}	11.430	0.550	0.072
π*	C_1—C_6	π*	C_2—C_3	235.750	0.010	0.079
σ*	S_7—N_{10}	π*	C_1—C_6	22.060	0.020	0.034
π*	N_{12}—C_{13}	π*	C_{14}—C_{15}	69.920	0.030	0.068
π*	N_{12}—C_{13}	σ*	C_{16}—F_{19}	9.780	0.160	0.066
π*	C_{14}—C_{15}	π*	C_{20}—C_{25}	90.210	0.010	0.048
π*	C_{20}—C_{25}	π*	C_{23}—C_{24}	271.050	0.010	0.080

[a] $E^{(2)}$ means energy of hyper conjugative interaction.
[b] Energy difference between donor and acceptor *i* and *j* NBO orbitals.
[c] $F(i,j)$ is the Fock matrix element between *i* and *j* NBO orbitals.

The other significant interactions giving stronger stabilization to the structure are $\pi^*(C_1—C_6) \rightarrow \pi^*(C_2—C_3)$, $\pi^*(C_{14}—C_{15}) \rightarrow \pi^*(C_{20}—C_{25})$ and $\pi^*(N_{12}—C_{13}) \rightarrow \pi^*(C_{14}—C_{15})$.

The Natural Localized Molecular Orbital (NLMO) analysis has been carried out since they show how bonding in a molecule is composed from orbitals localized on different atoms. The derivation of NLMOs from NBOs gives direct insight into the nature of the localized molecular orbital's "delocalization tails" [51]. Table 5 shows the significant NLMO's occupancy, percentage from parent NBO and atomic hybrid contributions of 4MPTFM1HPB1SA calculated at B3LYP level using 6-311++G(d,p) basis set. The NLMO of first lone pairs of Nitrogen atom N_{11} is the delocalized NLMO and has nearly 76% of contribution from the LP(1) N_{11} parent NBO and the delocalized tail (22%) consist of the hybrids of C_{15}, C_{13}, N_{12}, C_{14} and C_4. Similarly third lone pair O_8 has nearly 90% of contribution from LP(3) O_8 and the delocalized tail (9%) consists of S_7, N_{10} and O_9. The NLMOs of LP(3) O_9 have almost 9% delocalization tail. This delocalization can also be observed in the perturbation theory energy analysis as given in Table 5.

Table 5
NLMO analysis of 4MPTFM1HPB1SA.

Bond	Occupancy	Percentage from parent NBO	Hybrid contributions	
			Atoms	Percentage
LP(1)N_{11}	2.00000	75.5758	C_{15}	9.195
			C_{13}	4.856
			N_{12}	4.635
			C_{14}	2.137
			C_4	1.346
LP(3)O_8	2.00000	90.4711	S_7	5.125
			N_{10}	2.013
			O_9	2.011
LP(3)O_9	2.00000	90.7542	S_7	4.861
			O_8	2.178
			N_{10}	1.848
LP(3)F17	2.00000	96.3510	C_{16}	2.562
LP(2)O_8	2.00000	93.0071	S_7	3.422
			C_1	1.737
LP(2)O_9	2.00000	93.1549	S_7	3.258
			C_1	1.666

The Natural charge analysis

The Natural charges of 4MPTFM1HPB1SA obtained by Natural Bond Orbital analysis by B3LYP method with 6-311++G(d,p) basis set were listed in Table 6. The natural charges are shown in Fig. 4. The natural charges affect the dipole moment, polarizability, electronic structure and more a lot of properties of molecular systems. The natural charge distributions over the atoms suggest the formation of donor and acceptor pairs involving the charge transfer in the molecule [52]. The electronegative O_8, O_9, N_{10}, N_{11}, N_{12}, F_{17}, F_{18} and F_{19} atoms of compound 4MPTFM1HPB1SA have negative charge values. The natural charges of the mentioned atoms were calculated as −0.8079, −0.8109, −1.0393, −0.1809, −0.2388, −0.3410, −0.3534 and −0.3451 eV respectively. The C_4, S_7, C_{13}, C_{15}, C_{16}, H_{31} and H_{32} atoms bounded to the mentioned electronegative atoms in the molecule under study have positive charge values. The values of the positive charges of the mentioned atoms were found as 0.1586, 1.8304, 0.0006, 0.1675, 1.0541, 0.4262 and 0.4265 eV respectively. Therefore the C_{16} atom surrounded with three electronegative F_{17}, F_{18} and F_{19} atoms, and the S_7 atom surrounded with three electronegative O_8, O_9 and N_{10} atoms have the highest positive charge values. All the hydrogen atoms have positive charges. The maximum atomic charge is obtained for S_7 atom for when compared to other atoms. This is due to the attachment of negatively charged nitrogen and oxygen atoms. Negatively charged lone pair oxygen O_8, O_9 and nitrogen N_{10} atom shows that charge is transferred from O to S ($O_8 \rightarrow S_7$), ($O_9 \rightarrow S_7$) and N to S ($N_{10} \rightarrow S_7$). The maximum positive and negative charge is represented in S_7 and N_{10} atoms respectively.

UV–Visible studies and electronic properties

In an attempt to understand the nature of electronic transitions, positions of experimental absorption peaks, calculated absorption peaks (λ_{max}), vertical excitation energies(E), oscillator strengths (*f*) and assignments of the transitions of the 4MPTFM1HPB1SA

Table 6
The Natural charge analysis of 4MPTFM1HPB1SA molecule.

Atoms	Charges (eV)	Atoms	Charges (eV)
C_1	−0.2138	C_{21}	−0.2110
C_2	−0.2174	C_{22}	−0.2290
C_3	−0.2287	C_{23}	−0.0142
C_4	0.1586	C_{24}	−0.2336
C_5	−0.2152	C_{25}	−0.2095
C_6	−0.2172	C_{26}	−0.7162
S_7	1.8304	H_{27}	0.2843
O_8	−0.8079	H_{28}	0.2530
O_9	−0.8109	H_{29}	0.2821
N_{10}	−1.0393	H_{40}	0.2842
N_{11}	−0.1809	H_{31}	0.4262
N_{12}	−0.2388	H_{32}	0.4265
C_{13}	0.0006	H_{33}	0.2766
C_{14}	−0.2906	H_{34}	0.2714
C_{15}	0.1675	H_{35}	0.2492
C_{16}	1.0541	H_{36}	0.2472
F_{17}	−0.3410	H_{37}	0.2521
F_{18}	−0.3534	H_{38}	0.2477
F_{19}	−0.3451	H_{39}	0.2562
C_{20}	−0.1099	H_{40}	0.2558

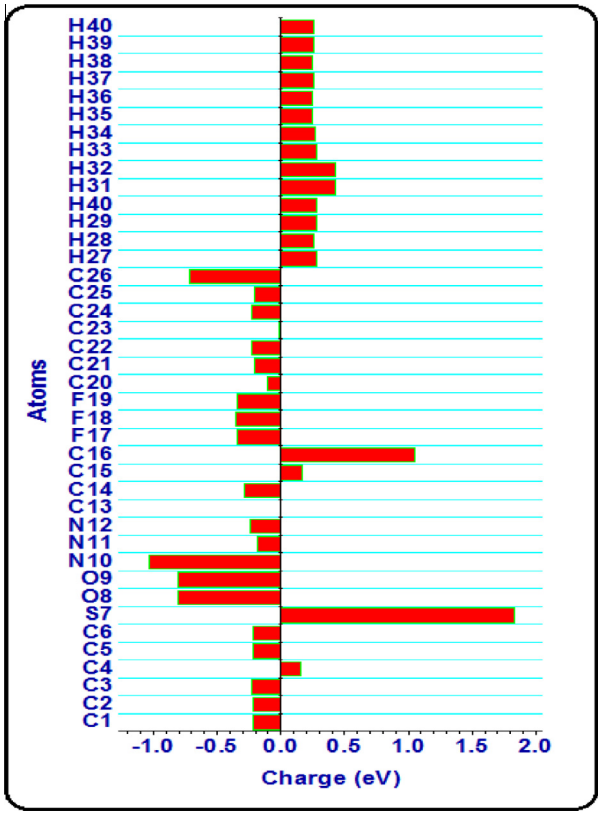

Fig. 4. Natural charge distribution in 4MPTFM1HPB1SA.

molecule were calculated and the results are presented in Table 7. The UV–Visible absorption spectrum of the title compound in DMSO solvent were recorded within the 200–400 nm range and representative spectrum is shown in Fig. 5.

The electronic absorption spectra were calculated using the TD-DFT method based on the B3LYP/6-311++G(d,p) level optimized structure in gas phase, water and acetone solution. For TD-DFT calculations, the theoretical absorption bands are predicted at 275.06, 253.26 and 252.59 nm in gas phase, 280.89, 254.81 and 253.44 nm in DMSO and 297.62, 265.05 and 261.74 nm in water solution. The TD-DFT calculations on electronic absorption spectra in water solvent were performed. The absorption wavelength is calculated at 297.62 nm is in good agreement with the experimental absorption wavelength at 294.00 nm in the UV–Visible spectrum [53–55].

Analysis of Frontier molecular orbitals

The Highest Occupied Molecular Orbitals (HOMOs) and Lowest Unoccupied Molecular Orbitals (LUMOs) are named as Frontier molecular orbital's (FMOs). The atomic orbital compositions of the frontier molecular orbital are shown in Fig. 6. The HOMO–LUMO energy gap of 4MPTFM1HPB1SA was calculated at B3LYP level with 6-311G(d,p) and 6-311++G(d,p) basis sets and is presented in Table 8. The LUMO as an electron acceptor represent the ability to obtain an electron, HOMO represents the ability to donate an electron [56–58]. The energy gap of HOMO–LUMO explains the eventual charge transfer interaction within the molecule, which influences the biological activity of the molecule. The positive and negative phase is represented in red and green color respectively. The energy of the two important FMOs such as the highest occupied molecular orbitals (HOMO), the lowest unoccupied molecular orbitals (LUMO) have been calculated.

The energy values of HOMO are 6.8203 and 6.9351 eV and the energy values of LUMO are 1.8991 and 2.0651 eV. The band gap between HOMO–LUMO are equal to 4.9212 and 4.8700 eV B3LYP method with 6-311G(d,p) and 6-311++G(d,p) basis sets respectively. The eigen values of HOMO, LUMO and energy gap between them can define kinetic stability. Also, energies of HOMO and LUMO are used for the determination of global reactivity descriptors. It is important that Ionization potential (I), Electron affinity (A), Electrophilicity (ω), Chemical potential (μ), Electronegativity (χ), Hardness (η) and Softness (S) be put into a MO framework. We focus on the HOMO and LUMO energies in order to determine the interesting molecular/atomic properties and chemical quantities.

In simple molecular orbital theory approaches, the HOMO energy is related to the ionization potential (I) and the LUMO energy has been used to estimate the electron affinity (A) respectively by the following relations:

$I = -E_{\mathrm{HOMO}}$ and $A = -E_{\mathrm{LUMO}}$.

The chemical potential of the molecule is $(\mu) = -(I + A)/2$.
The absolute hardness of the molecule is $(\eta) = (I - A)/2$.
The softness is the inverse of the hardness $(S) = 1/\eta$.
The electronegativity of the molecule is $(\chi) = (I + A)/2$.
The electrophilicity index of the molecule is $(\omega) = \mu^2/2\eta$.

The quantum chemical parameters of the molecule are presented in Table 8. Gauss-Sum 2.2 program [59] was used to calculate the group contributions to the molecular orbital (HOMO and LUMO) and to prepare the density of states (DOS) spectrum as shown in Fig. 7. The DOS spectra were created by convoluting the molecular orbital information with the Gaussian curves of unit height. The green and blue lines in the DOS spectrum indicate the HOMO and LUMO levels respectively.

Molecular electrostatic potential surface

The molecular electrostatic potential surface (MESP) is a plot of electrostatic potential mapped on to the constant electron density surface. The MESP superimposed on top of the total energy density as a shell. Because of the usefulness feature to study reactivity given that an approaching electrophilic will be attracted to negative regions. In majority of the MESP the maximum negative region which the preferred the site for electrophilic attack is indicated in

Table 7
Wavelength (nm), oscillatory strength (*f*) and energy (eV) of 4MPTFM1HPB1SA.

Calculated with B3LYP/6-311++G(d,p)									Exp
Gas phase			DMSO			Water			
λ_{max} (nm)	*E* (ev)	*f*	λ_{max} (nm)	*E* (ev)	*f*	λ_{max} (nm)	*E* (ev)	*f*	λ_{max} (nm)
275.06	4.5075	0.0750	280.89	4.4140	0.0871	297.62	4.1659	0.1250	294.00
253.26	4.8956	0.3462	254.81	4.8657	0.3097	265.05	4.6778	0.0619	
252.59	4.9085	0.0058	253.44	4.8920	0.1222	261.74	4.7369	0.2649	

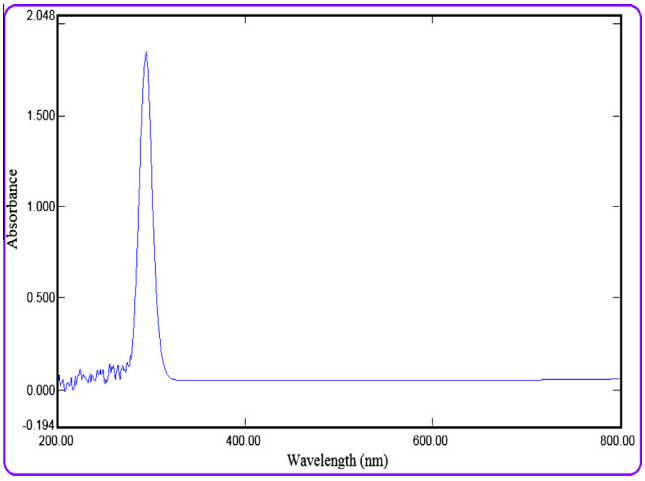

Fig. 5. Observed UV–Visible spectrum of 4MPTFM1HPB1SA.

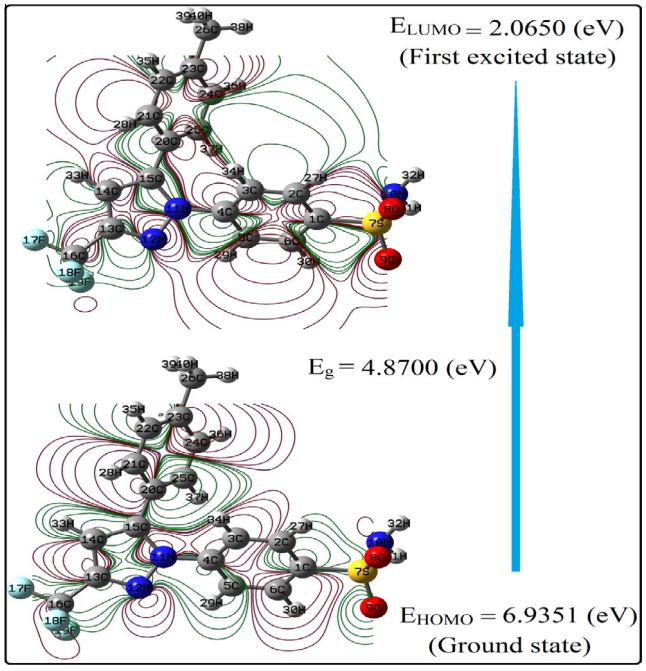

Fig. 6. HOMO and LUMO plots of 4MPTFM1HPB1SA.

as red color, while the maximum positive region which preferred the site for nucleophilic attack is symptoms indicated in blue color [60]. The computationally observed MESP surface map with the fitting point charges to the electrostatic potential for the title compound. The purpose of finding the electrostatic potential is to find the reactive site of a molecule. These maps allow us to visualize variably charged regions of a molecule. Knowledge of the charge distributions can be used to determine how molecules interact with one another.

The different values of the electrostatic potential at the surface are represented by different colors. Potential increases in the order red < yellow < green < light blue < blue. The color scheme for the MESP surface is red-electron rich, partially negative charge; yellow-slightly electron rich region; green-neutral; light blue-slightly electron deficient region and blue-electron deficient, partially positive charge respectively. Areas of low potential red are characterized by an abundance of electrons. Areas of high potential blue are characterized by the relative absence of electrons. Such mapped electrostatic potential surfaces have been plotted for 4MPTFM1HPB1SA in B3LYP/6-311++G(d,p) method using the computer software Gauss view 5.0.

The molecular electrostatic potential countour surface of 4MPTFM1HPB1SA is shown in the Fig. 8. The total electron density surface mapped with the molecular electrostatic potential of 4MPTFM1HPB1SA is shown in Fig. 9. The importance of MESP lies in the fact that it simultaneously displays molecular size, shape, positive as well as negative and neutral electrostatic potential regions in terms of color grading and is very useful in the research of molecular structure with its physicochemical property relationship. The color code of the map is between −0.0790 a.u. (red) to 0.1190 a.u. (blue) for the compound, where blue indicates the strongest attraction and red indicates the strongest repulsion [61,62]. The MESP map shows the negative potential sites are on oxygen, fluorine and nitrogen atoms as well as the positive potential sites are around the hydrogen atoms.

Table 8
HOMO, LUMO, HOMO–LUMO energy gap and physico-chemical properties of 4MPTFM1HPB1SA.

Parameters (eV)	B3LYP/6-311G(d, p)	B3LYP/6-311++G(d, p)
HOMO Energy	6.8203	6.9351
LUMO Energy	1.8991	2.0651
HOMO–LUMO Energy gap	4.9212	4.8700
Ionization potential (*I*)	−6.8203	−6.9351
Electron affinity (*A*)	−1.8991	−2.0651
Global hardness (η)	2.4606	2.4350
Global softness (S)	0.4064	0.4106
Chemical potential (μ)	−4.3597	−4.5001
Electrophilicity (ω)	3.8622	4.1583
Electro negativity (χ)	4.3597	4.5001

Thermodynamic properties

The values of some thermodynamic parameters (such as zero-point vibrational energy, thermal energy, specific heat capacity, rotational constants and entropy) of 4MPTFM1HPB1SA at 298.15 K in ground state were calculated by B3LYP methods with 6-311G(d,p) and 6-311++G(d,p) basis set and were listed in Table 9. The variation in Zero-Point Vibrational Energies (ZPVEs) seems to be significant. The ZPVE is lower by the B3LYP with 6-311++G(d,p) basis set than by the B3LYP with 6-311G(d,p) basis set. The calculated values of ZPVE of 4MPTFM1HPB1SA are 181.60 kcal/mol and 181.87 kcal/mol obtained by B3LYP with 6-311++G(d,p) and 6-311G(d,p) basis sets respectively [63].

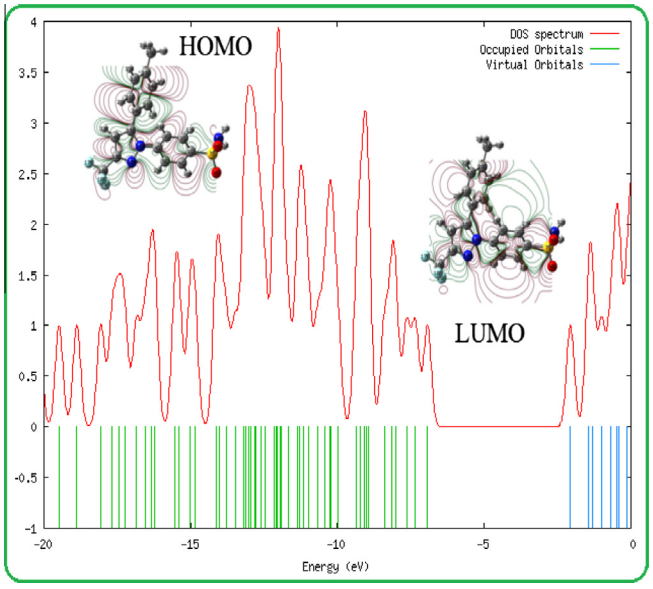

Fig. 7. Density of state (DOS) spectrum of 4MPTFM1HPB1SA.

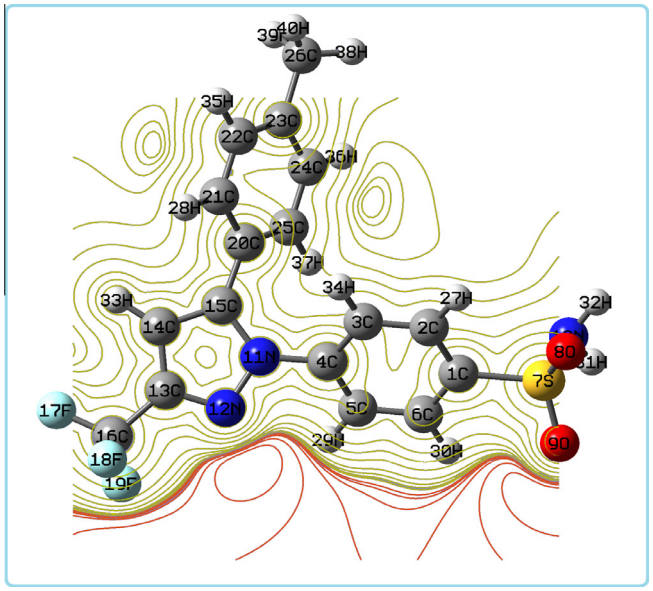

Fig. 8. Molecular electrostatic potential contour surface of 4MPTFM1HPB1SA.

The biggest value of thermal energy is 196.60 kJ mol^{-1} obtained at B3LYP/6-311G(d,p) method. As a result of B3LYP with 6-311G(d,p) and 6-311++G(d,p) calculations, the highest entropy was calculated as 172.27 cal/mol $^{-1}K^{-1}$ at B3LYP with 6-311G(d,p) basis set, whereas the smallest one was observed as 172.10 cal/$mol^{-1}K^{-1}$ at B3LYP/6-311++G(d,p) in 4MPTFM1HPB1SA. However, specific heat capacity and entropy were calculated, the smallest and highest values were obtained by B3LYP/6-311G(d,p) and B3LYP/6-311++G(d,p) respectively.

On the basis of vibrational analysis at B3LYP level with 6-311G(d,p) and 6-311++G(d,p) several standard statistical thermodynamic functions, viz., heat capacities ($C^0_{p,m}$), entropies (S^0_m) and enthalpy (H^o_m) changes for the title compounds have been obtained on the basis of vibrational analysis and statistical thermodynamics [64]. The correlations between the thermodynamic properties and temperature are shown in Fig. 10 and listed in Table 9. From the figure it can be observed that the heat capacities,

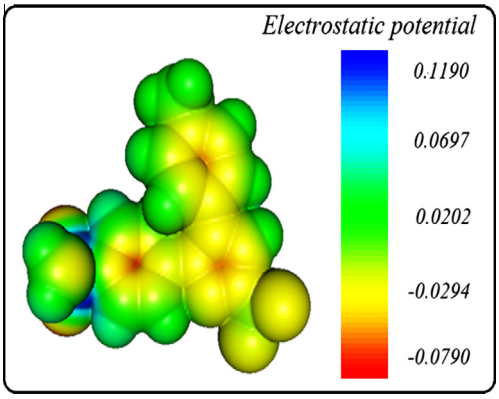

Fig. 9. Molecular electrostatic potential surface of 4MPTFM1HPB1SA.

Table 9
Calculated thermodynamic parameters of 4MPTFM1HPB1SA.

Parameter	B3LYP/6-311G(d,p)	B3LYP/6-311++G(d,p)
Zero-point		
Vibrational energy (kJ/mol)	181.87	181.60
Rotational constant (GHz)	0.20	0.20
	0.11	0.11
	0.08	0.08
Thermal energy (kJ/mol)		
Total	196.60	196.33
Translational	0.89	0.89
Rotational	0.89	0.89
Vibrational	194.82	194.55
Heat capacity constant (cal/mol^{-1} K^{-1})		
Total	87.75	87.90
Translational	2.98	2.98
Rotational	2.98	2.98
Vibrational	81.79	81.94
Entropy (cal/mol^{-1} K^{-1})		
Total	172.27	172.01
Translational	43.71	43.71
Rotational	36.46	36.46
Vibrational	92.10	91.84

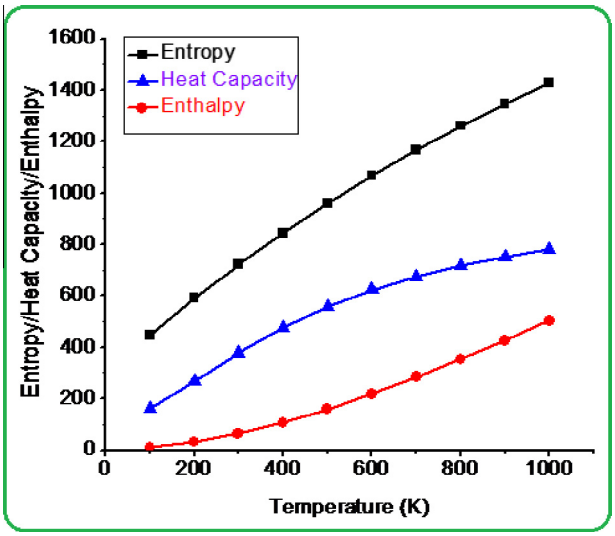

Fig. 10. Thermodynamic properties of 4MPTFM1HPB1SA.

entropies and enthalpy changes are increasing with temperature ranging from 100 to 1000 K. This is due to the fact that the molecular vibrational intensities increase with increase in temperature.

Table 10
Thermodynamic properties at different temperatures at B3LYP/6-311G++(d,p) level for 4MPTFM1HPB1SA.

T (K)	S (cal mol^{-1} K^{-1})	C (cal mol^{-1} K^{-1})	ΔH (k cal mol^{-1})
100.00	446.42	164.32	10.75
200.00	592.19	269.67	32.38
298.15	719.78	376.10	64.09
300.00	722.11	378.06	64.79
400.00	844.79	477.06	107.67
500.00	960.37	558.88	159.62
600.00	1068.24	623.79	218.88
700.00	1168.41	675.22	283.93
800.00	1261.37	716.58	353.59
900.00	1347.79	750.42	427.00
1000.00	1428.35	778.51	503.49

These empirical relations of the thermodynamic functions vs temperature were fitted by quadratic formulas and the corresponding fitting regression factors (R^2) for these thermodynamic properties are 0.9994, 0.9999 and 0.9992 respectively.

$$C^0_{p,m} = 31.8644 + 1.3417T - 5.9947 \times 10^{-4}T^2 \quad (R^2 = 0.9994)$$

$$S^0_m = 303.4811 + 1.5054T - 3.8270 \times 10^{-4}T^2 \quad (R^2 = 0.9999)$$

$$H^0_m = -17.4324 + 0.1852T + 3.4123 \times 10^{-4}T^2 \quad (R^2 = 0.9992)$$

All the thermodynamic data supply helpful information for the further study on the 4MPTFM1HPB1SA. They can be used to compute the other thermodynamic energies according to relationships of thermodynamic functions and estimate the directions of chemical reactions according to the second law of thermodynamics in thermo chemical field.

Notice: all thermodynamic calculations were done in gas phase and they could not be used in solution (See Table 10).

Conclusion

The FT-IR and FT-Raman have been recorded and the detailed vibrational assignment is presented for 4MPTFM1HPB1SA for the first time. A complete vibrational investigation of the title compound has been performed using FT-IR and Raman spectroscopic techniques and the various modes of vibrations were explicitly assigned on the results of PED analysis. The equilibrium geometries, harmonic frequencies, infrared intensities and Raman scattering activities of the molecule were determined and analyzed by B3LYP with 6-311G(d,p) and 6-311++G(d,p) basis sets. The simulated FT-IR and Raman spectra of the title compound show good agreement with the observed spectra. The electric dipole moment, polarizability, mean polarizability and the first order hyperpolarizability of the title compound were calculated. The stability and intramolecular interactions have been interpreted by NBO/NLMO analysis and the transactions give stabilization to the structure have been identified by second order perturbation energy calculations. The natural atomic charges of the title molecule have been studied by DFT methods. Absorption maxima (λ_{max}) of 4MPTFM1HPB1SA was calculated by TD-DFT method and compared with the experimental UV–Visible spectra. Increased HOMO and LUMO energy gap explains the eventual charge transfer within the molecule which is responsible for the chemical reactivity of the molecule. HUMO and LUMO orbitals have been visualized. It has been conclude that the lowest singlet excited state of the title molecule is mainly derived from the HOMO → LUMO electron transition. The MESP map shows the negative potential sites are on oxygen, nitrogen and fluorine atoms as well as the positive potential sites are around the hydrogen atoms. The correlations of the statistical thermodynamics according to temperature were also presented.

References

[1] S. Lavakumar, K. Lahon, J. Pandian, Int. J. Pharm. Bio. Sci. 4 (2013) 976–984.
[2] G. Chawla, P. Gupta, R. Thilagavathi, A. Chakraborti, A. Bansal, Eur. J. Pharm. Sci. 20 (2003) 305–317.
[3] F. Leonard, F. Patricia, Polymorphic crystalline forms of 4MPTFM1HPB1SA. WO 01/42222, 2001.
[4] M. Jozwiakowski, Interpharm Press, Colorado, 2000, pp. 525–562.
[5] G. Van den Mooter, M. Wuyts, N. Blaton, Eur. J. Pharm. Sci. 12 (2001) 261–269.
[6] S. Esnaashari, Y. Javadzadeh, H.K. Batchelor, B.R. Conway, Int. J. Pharm. 292 (2005) 227–230.
[7] A. Salim, E. Moghimipour, N. Tavakolbekhoda, Int. Res J. Pharm. Appl. Sci. 3 (4) (2013) 173–181.
[8] H.J. Frisch, G.W. Trucks, H.B. Schlegel, G.E. Scuseria, M.A. Robb, J.R. Cheeseman, H. Nakatsuji, M. Caricato, X. Li, H.P. Hratchian, K. Toyota, R. Fukuda, J. Hasegawa, M. Ishida, R. Nakajima, Y. Honda, O. Kilao, H. Nakai, T. Verven, J.A. Montgomery Jr., J.E. Peralta, F. Ogliaro, M. Bearpark, J.J. Heyd, E. Brothers, K.N. Kudin, V.N. Staroveror, R. Kobayashi, J. Normand, K. Ragavachari, A. Rendell, J.C. Burant, S.J. Tomasi, M. Cossi, N. Rega, J.M. Millam, M. Klene, J.E. Knox, J. B. Cross, V.Bakken, C. Adamo, J. Jaramillo, R. Gomperts, R.E. Strattmann, O. Yazyev, A.J. Austin, R. Cammi, J.W. Ochetrski, R.L. Martin, K. Morokuma, V.G. Zakrazawski, G.A. Votn, P. Salvador, J.J. Dannenberg, S. Dapprich, A.D. Daniels, O. Farkas, J.B. Foresman, Gaussian O.G., Revision A.O2, Gaussian Inc., Wallingford, CT, 2009.
[9] A.D. Becke, J. Chem. Phys. 98 (1993) 5648–5652.
[10] C. Lee, W. Yang, R.G. Parr, Phys. Rev. B37 (1998) 785–789.
[11] A. Frisch, A.B. Nielson, A.J. Holder, GAUSSVIEW User Manual, Gaussian Inc., Pittsurgh PA, 2000.
[12] M.H. Jamroz, Vibrational energy Distribution Analysis VEDA 4, Warsaw, Poland, 2004.
[13] W.J. Hehre, L. Radom, P.V.R. Schleyer, J.A. Pople, Ab initio Molecular Orbital Theory, Wiley, New York, 1986.
[14] C. Herrmann, M. Reiher, Top. Curr. Chem. 268 (2007) 85–132.
[15] E.D. Glendening, J.K. Badenhoop, A.E. Reed, J.E. Carpenter, J.A. Bohmann, C.M. Morales, F. Weinhold, NBO 5.0, Theoretical Chemistry Institute, University of Wisconsin, Madison, 2001.
[16] A.M. Asiri, A.O. Al-Youbi, H.M. Faidallah, S.W. Ng, E.R.T. Tiekink, Acta Cryst. E 67 (2011) S1–S6.
[17] S.P. Vijaya Chamundeeswari, E. James Jebaseelan Samuel, N. Sundaraganesan, Spectrochim. Acta Part A Mol. Biomol. Spectrosc. 118 (2014) 1–10.
[18] B. Lambert, Introduction to Organic Spectroscopy, Macmillan Publjcation, New York, 1987.
[19] M. Tsuboi, Spectrochim. Acta A 16 (1960) 505–512.
[20] N.P.G. Roges, A Guide to the Complete Interpretation of Infrared Spectra of Organic Structures, Wiley, New York, 1994.
[21] V. KrishnaKumar, N. Prabavathi, Spectrochim. Acta A 72 (2009) 738–742.
[22] R.L. Peesole, L.D. Shield, I.C. McWilliam, Modern Methods of Chemical Analysis, Wiley, New York, 1976.
[23] Y.R. Sharma, Elementary Organic Spectroscopy-Principles and Chemical Applications, S. Chande & Company Ltd., New Delhi, 1994.
[24] M. Silverstein, G. Clayton Basseler, C. Morill, Spectrometric Identification of Organic Compound, Wiley, NewYork, 1981.
[25] G. Socrates, Infrared Characteristic Group frequencies, Wiley-Interscience Publication, New York, 1980.
[26] S. George, Infrared and Raman Characteristic Group Wavenumbers, Tables and Charts, third ed., Wiley, Chichester, 2001.
[27] D. Lin-Vien, N.B. Colthup, W.G. Fateley, J.G. Graselli, The Hand Book of Infrared and Raman Characteristic Frequencies of Organic Molecules, Academic Press, New York, 1991.
[28] G. Varsanyi, Assignments of Vibrational Spectra of 700 Benzene Derivatives, Wiley, New York, 1974.
[29] S. Gunasekaran, P. Arunbalaji, S. Seshadri, S. Muthu, Indian J. Pure Appl. Phys. 46 (2008) 162–168.
[30] D. Shoba, S. Periandy, M. Karabacak, S. Ramalingam, Spectrochim. Acta Part A Mol. Biomol. Spectrosc. 83 (2011) 540–552.
[31] C. James, C. Ravikumar, V.S. Jayakumar, I. Hubert Joe, J. Raman Spectrosc. 40 (2009) 537–545.
[32] S. Pinchas, D. Samuel, M. Weiss-Broday, J. Chem. Soc. (1961) 1688–1691.
[33] L. Kahovec, K.W.F. Kohlreusch, Monatsh. Chem. 74 (1941) 333–343.
[34] H. Gokce, O. Akyildirim, S. Bahceli, H. Yuksek, O. Gursoy Kol, J. Mol. Struct. 1056–1057 (2014) 273–284.
[35] N.G.P. Roeges, A Guide to the Complete Interpretation of the Infrared Spectra of Organic Structures, Wiley, NY, 1994.
[36] A. Hangen, A. Bodoki, L. Opren, G. Alznet, M.L. Gonzalez, J. Borras, Polyhedron 29 (2010) 1305–1313.
[37] A. Rodriguez, M.E.S. Vergara, V.G. Montalvo, A.O. Rebollo, J.R.A. Bada, C.A. Toledano, Spectrochim. Acta 75 (2010) 479–485.
[38] M. Arivazhagan, D. Anitha Rexalin, G. Ilango, Spectrochim. Acta A 121 (2014) 641–649.
[39] P.J.A. Ribeiro-Claro, M.P.M. Marques, A.M. Amado, ChemPhysChem 3 (2002) 599–606.

[40] N.B. Colthup, L.H. Daly, S.E. Wiberley, Introduction to Infrared and Raman Spectroscopy, Academic Press, New York, 1990.
[41] C.S. Hsu, Spectroscop. Lett. 7 (9) (1974) 439–447.
[42] R. Zhang, B. Dub, G. Sun, Y. Sun, Spectrochim. Acta A 75 (2010) 1115–1124.
[43] D.A. Kleinman, Phys. Rev. 126 (1962) 1977–1979.
[44] O. Christiansen, J. Gauss, J.F. Stanton, J. Chem. Phys. Lett. 305 (1999) 147–155.
[45] R.T. Lynch Jr., M.D. Levenson, N. Bloembergen, Phys. Lett. 50 (1974) 61–62.
[46] S. Ramalingam, M. Karabacak, S. Periandy, N. Puviarasan, D. Tanuja, Spectrochim. Acta Part A Mol. Biomol. Spectrosc. 96 (2012) 207–220.
[47] C. James, A. AmalRaj, R. Reghunathan, J. Raman Spectrosc. 37 (2006) 1381–1392.
[48] L.J. Na, C.Z. Rang, Y.S. Fang, J. Zhejiang, Univ. Sci. B 6 (2005) 584–589.
[49] M. Szafram, A. Komasa, E.B. Adamska, J. Mol. Struct. 827 (2007) 101–107.
[50] A.E. Reed, P.V.R. Schleye, Inorg. Chem. 27 (1988) 3969–3987.
[51] R.R. Saravanan, S. Seshadri, S. Gunasekaran, R. Mendoza-Meroño, G. Garcia-Granda, Spectrochim. Acta Part A 121 (2014) 268–275.
[52] R. John Xavier, E. Gobinath, Spectrochim. Acta Part A Mol. Biomol. Spectrosc. 97 (2012) 215–222.
[53] D. Shoba, S. Periandi, S. Boomadevi, S. Ramalingam, E. Fereyduni, Spectrochim. Acta Part A Mol. Biomol. Spectrosc. 118 (2014) 438–447.
[54] M. Govindarajan, M. Karabacak, S. Periandy, D. Tanuja, Spectrochim. Acta Part A 97 (2012) 231–245.
[55] M. Govindarajan, M. Karabacak, Spectrochim. Acta Part A 101 (2013) 314–324.
[56] R.S. Mulliken, J. Chem. Phys. 2 (1934) 782.
[57] I. Lukovits, I. Bako, A. Shaban, E. Kalman, Electrochim. Acta 43 (1998) 131–136.
[58] R.G. Parr, L.V. Szentpaly, S. Liu, J. Am. Chem. Soc. 121 (1999) 1922–1924.
[59] E.D. Glendening, C.R. Landis, F. Weinhold, WIREs Comput. Mol. Sci. 2 (2011).
[60] P. Politzer, J.S. Murray, Theor. Chem. Acc. 108 (2002) 134–142.
[61] F.J. Luque, J.M. Lopez, M. Orozco, Theor. Chem. Acc. 103 (2000) 343–345.
[62] N. Okulik, A.H. Jubert, J. Mol. Des. 4 (2005) 17–30.
[63] D. Sajan, L. Josepha, N. Vijayan, M. Karabacak, Spectrochim. Acta Part A Mol. Biomol. Spectrosc. 81 (2011) 85–98.
[64] R. Zhang, B. Dub, G. Sun, Y. Sun, Spectrochim. Acta Part A Mol. Biomol. Spectrosc. 75 (2010) 1115–1124.